Structural characterization of electro-thermally driven micro-actuators with immeasurable temperature-dependent material characteristics

W. Szyszkowski & D. Hill
Department of Mechanical Engineering, University of Saskatchewan, Canada

Abstract

Multi-cell cascaded Electro-Thermal Micro-Actuators (ETMA) made of nickel alloys are analyzed by the finite element (FE) method. The computer simulation runs over the electrical, thermal, and mechanical phases of the ETMA operations. The main challenges of modeling are discussed. Some of the material's parameters such as the electrical resistivity, thermal expansion coefficient and emission are strongly temperature dependent. Furthermore, any measurements of such dependences are complicated by a magnetic phase transition occurring in nickel within the operating range of temperature. All the properties are sensitive to a particular composition of the material. The surface convection is additionally shape-dependent and, mainly due to small dimensions of the actuators, cannot be determined experimentally with sufficient accuracy. For the above reasons the use of the material data estimated from the available literature usually does not render reliable simulations.

In the approach proposed the material characteristics of the ETMA considered are determined by utilizing the fact that for a given applied voltage the total current and displacement in the real actuators (performance parameters) are measured with a relatively high precision. Similar performance parameters, i.e. the total current and displacement can be obtained as output from the FE simulation in which some important material properties of the actuator's model are assumed in a parametric form (material's parameters). The FE simulation procedure is integrated with these real measurements in such a way that the

material parameters are iteratively adjusted to match the simulated and experimental performance parameters for the sampled actuators.

Keywords: micro-actuators, finite elements, electro-thermal-mechanical fields, uncertain material characteristics.

1   Introduction

Electro-thermal micro-actuators (ETMA) are constructed as monolithic compliant mechanisms. They have the displacement/force outputs typically higher than other micro-actuators, and should be easier to control [1, 2]. However, mainly due to relatively high temperatures of the operating regimes [3, 4], any analytical predictions and numerical simulations are rather challenging. Several parameters to characterize three different physical environments involved, i.e. electrical, thermal, and mechanical, may vary quite substantially over the temperature ranges the actuators usually experience.

While the finite element (FE) technique is capable of handling complicated geometrical shapes, obtaining data and modeling these material parameters for a particular ETMA remains difficult and seems to be the main source of the discrepancies between the computed and measured results. Some of the parameters are also scale dependent and almost impossible to measure for such small devices, or may be affected by the changes in the material's microstructure triggered at some transition temperatures difficult to detect with a sufficient precision. Consequently, analytical predictions of the structural characteristics of such devices have not been particularly accurate so far, and that's why any new designs still have to rely heavily on costly, time consuming, and numerous experimental testing.

Most of the FE analysis of ETMA reported in the literature adopted the material parameters as temperature-independent constants at best 'averaged' over the expected operating temperature range [5, 6], while in fact their values may vary several times over that range.

The above issues are discussed here on the example of cascaded ETMA made of nickel alloy and manufactured by using laser micro-fabrication technology [7]. All the main material parameters are assumed temperature-dependant. The material's description is assessed by comparing the ETMA's measured and the FE simulated performance parameters. In order to improve accuracy the FE simulation is combined with experimental testing to modify the values of some uncertain material parameters. The procedure is iterative in which the changes in temperature distribution, indicating the coupling between the electrical and thermal fields, and the ETMA performance, which is sensitive to the current values of the material parameters, are monitored. It is demonstrated that only the measurements pertaining to the electrical and mechanical fields are needed, while rather cumbersome, unreliable, or just impossible measurements of the heat transfer and temperatures can be avoided.

2   The ETMA and the governing equations

The multi-cascaded ETMA of the overall dimensions shown in Figure 1a was manufactured from a 25μm thick nickel alloy foil by a laser-material removal process [7]. An application of two actuators to drive micro-tweezers is sketched in Figure 1b. Each actuation unit, which has a fixed electrical anchor to apply power to, consists of several *actuation cells* connected serially. The cell is composed of two actuation beams to be referred to as *hot arms*, and one constraining beam to be referred to as a *constrainer*. Electro-thermal micro-actuators utilize the effects of thermal expansion of metals upon heating due to electrical current when voltage V_a is applied. The thermal expansion is to be converted into either the vertical displacement u of the motion platform, or the force F, or both. For best effects, the temperature field should be such that hot members expand as freely as possible, while the thermal expansion in constrainers is reduced as much as possible. These requirements are not easy to meet, because both the thermal and structural effects in hot arms and constrainers are coupled.
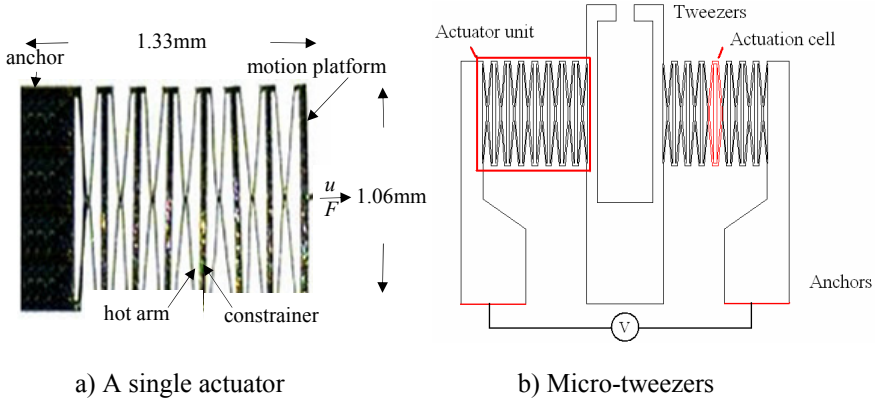

| a) A single actuator | b) Micro-tweezers |

Figure 1:   Multi-cell cascaded ETMA.

The distributions of voltage V, current density i, and power Q in the actuator are governed by the equations:

$$\nabla \cdot (\tfrac{1}{\rho}\nabla V) = 0$$
$$i = -\rho \nabla V \qquad\qquad (1a,b,c)$$
$$Q = \tfrac{1}{\rho}\nabla V \nabla V$$

where $\rho(T)$ is a temperature dependent resistivity of the material.

Power Q is converted into Joule's heat generated per unit of the volume. The temperature raise, T, is governed by the equations representing the heat transfer via conduction in the body and through convection/radiation on the surface in the form:

$$\nabla(K\nabla T) + Q = 0 \qquad\qquad (2a,b)$$

$$KVT + h(T - T_0) + eB(T^4 - T_0^4) = 0$$

where $K(T)$, $h(T)$, and $e(T)$ are the temperature-dependant conduction, convection, and emissivity coefficients respectively.

Finally, the stress/strain/displacement (denoted by σ, ε, and u respectively) field is governed by equilibrium, constitutive law, and kinematics equations in the form:

$$\sigma_{ij,j} + f_i = 0$$

$$\sigma_{ij} = D_{ijkl}(\varepsilon_{kl} - \alpha \Delta T \delta_{kl}) \tag{3abc}$$

$$\varepsilon_{ij} = \tfrac{1}{2}(u_{i,j} + u_{j,i})$$

where D_{ijkl} is defined in terms of the temperature-dependent elasticity modulus $E(T)$ and Poisson's ratio $v(T)$, while $\alpha(T)$ is the thermal expansion coefficient.

As can be seen from equations (1) and (2), the temperature T and the voltage V distributions are both affected by the power Q effectively coupling the electrical and thermal fields. To analyze these two phases the following material parameters are required $\rho(T)$, $K(T)$, $h(T)$, and $e(T)$. Once the temperature is determined the corresponding stress/deformations can be obtained. In this final phase only $E(T)$ and $v(T)$ have to be known.

The temperature in the actuator considered varies from point to point within the range of about 20-600°C. As discussed in the next section, some of the above parameters may vary quite substantially over that range. Also, the convection coefficient, which varies the most, is generally almost impossible to obtain from experimental measurements.

3 Effects of temperature on the material characteristics

Although nickels alloys are popular materials used in microelectronics, no data were available for the alloys matching exactly the material used in this particular ETMA (90% Nickel, 6% Copper, and 4% trace materials). However, the published data [8–11] for similar compositions have generally indicated the following:
- The resistivity and the convection coefficients are affected by temperature much more than the other parameters.
- In particular the temperature dependence of the resistivity is highly sensitive to material composition.
- Within the temperature range of the ETMA operations a magnetic phase change may occur in the material, which will affect its properties.

Another important factor is that the convection coefficient is also strongly shape-dependent, which means, for example, that it should be measured on 'micro-samples' of the geometry similar to the geometry of the hot arm ($0.010 \times 0.025\ mm$ rectangle), the task that practically appears to be almost impossible.

A 'macro-sample' of dimensions $22 \times 6 \times 0.025\ mm$ kept at a uniform temperature was used to determine the resistivity and emissivity. The

temperature was measured with the help of a hot plate and thermal glasses. It was found that the resistivity varies quadratically with temperature up to about 306ºC, above this temperature the variation is linear. It was concluded that this is due to the phase change that takes place at $T_p = 306\,°C$. The following relationship was used in the FE simulation (SI units are used):

$$\rho(T) = \begin{cases} 6.77 \cdot 10^{-5} \cdot (1 + 0.00476T(1 + 0.00303T)) & if \quad T \le 306 \\ 16.4 \cdot 10^{-5} \cdot (1 + 0.001872T) & if \quad T > 306 \end{cases} \quad \text{(4a,b)}$$

In should be noticed that the magnitude of $\rho(T)$ changes by some 420% over the range of 20–600ºC.

The emissivity was found to vary pretty much linearly with temperature. The variation was approximated by:

$$e(T) \cong 0.1 \cdot (1 + 0.0008T) \quad \text{(5)}$$

Note that the magnitude of this parameter varies only about 50% over the same range of temperature.

According to [10], variation of the thermal conduction coefficient should be less significant over that temperature range. Typically its value first slightly drops with temperature, and then starts to increasing, the change most probably associated with the magnetic phase change already mentioned.

$$K(T) = \begin{cases} 92.4 - 0.093T & if \quad T < 306 \\ 56.3 + 0.025T & if \quad T > 306 \end{cases} \quad \text{(6)}$$

It should be noted that this coefficient varies about 30% over the whole temperature range.

The relations $h(T)$ is more difficult to establish. This is because generally the convection coefficient dependents on the geometry of heat transferring body. On the other hand, any direct temperature or heat flux measurements on a 'micro-sample' with the dimensions comparable to the hot arms dimensions are very challenging (too small for thermal glasses, for example). Nevertheless the 'macro-sample' mentioned above was used to determine this coefficient as well. The results are denoted by the curve $h_t(T)$ shown in Figure 2. This curve is generally in a range for a flat surface undergoing free convection [12]. Note that for this test the value of the convection coefficient changed about 8 times over the temperature range from 20ºC to 600ºC.

What was the most important, however, was that $h_t(T)$ used in the FE simulation were giving consistently much *higher* then expected temperature of the hot arms (around 2400ºC), which in turn indicated that the convection coefficient for small dimensions members of the actuator should be much higher than those obtained for a relatively flat surface of the macro-sample. However, it was noticed that the convection coefficient data for small diameter wires

published in [12] are generally of similar character, but numerical values were higher. For example, for the wire of $100\mu m$ this coefficient, denoted by $h_w(T)$ in Figure 2, is about 5 times higher than $h_t(T)$. Also, one should realize that the convection coefficient values shown in Figure 2 vary about 10 times over the temperature range of 20-600ºC.
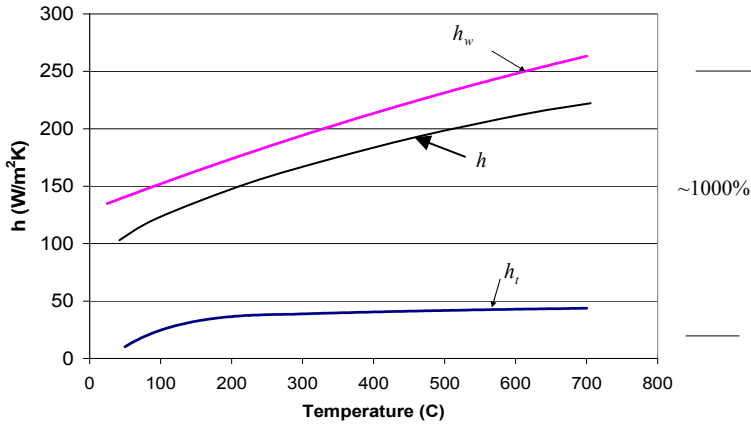

Figure 2:   The convection coefficient.

When the curve $h_w(T)$ was used in the ETMA's simulation, the resulting temperature was in turn *lower* than expected. It indicated, when combined with the numerical test performed on $h_t(T)$, that for the members of the actuator the convection coefficient $h(T)$ should be limited by $h_t < h < h_w$. Therefore this coefficient is assumed in the form:

$$h(T) = \eta h_w + (1 - \eta)h_t, \tag{7}$$

where the value of parameter η is to be determined by comparing the simulation and experimental results.

The mechanical properties such as Young's modulus, E, and Poisson's ratio v, as well as the thermal expansion coefficient α are less affected by the temperature and the alloy composition.

The variation of E with temperature up to 600ºC were adopted from [8] in the form:

$$E(T) = 206.4 \cdot 10^9 \cdot (1 - 0.000286T) \tag{8}$$

The Poisson's ratio v, according to [11], can be considered approximately constant and equal to 0.31.

Reference [8] also suggested the linear variation of α with temperature as:

$$\alpha(T) = 13 \cdot 10^{-6}(1 + 0.000343T) \tag{9}$$

However, the detailed data reported in [13,14] for a similar Nickel alloy shown that α increased with temperature up to the magnetic phase transition, then dropped down, and started increasing again for temperatures above

approximately 450°C. The data as well as the linear formula (11) are plotted in Figure 3. In the FE simulation the $\alpha(T)$ relation is approximated by piecewise linear functions also indicated in Figure 3, with the parameters $\alpha_0, \alpha_1, \alpha_2, \alpha_3, T_1, T_2$, and T_3. The values of these parameters indicated in this figure were determined by matching the simulation and experimental displacement results as closely as possible, as explained in the next section.
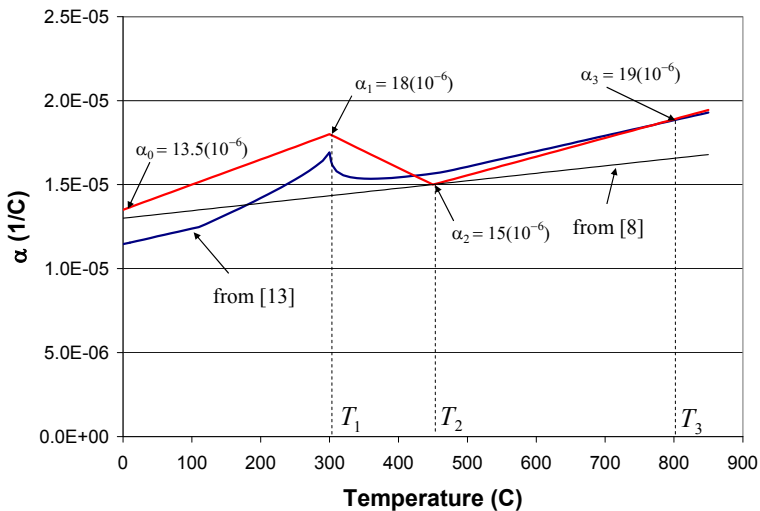

Figure 3:   The thermal expansion coefficient.

Note that for the temperature range considered the values of $E(T)$ or $\alpha(T)$ parameters change only about 20%. Therefore any inaccuracies in these properties should have much less effects on the response of the simulated actuator than the inaccuracies in the convection or resistivity coefficients.

4   The FE modeling and simulation procedure

The finite element simulation of the cascaded actuation unit would have to depict accurately the response of the system across three main physics environments; electrical, thermal and mechanical. The flow chart in Figure 4 outlines the main blocks of the analysis. The complete simulation procedure was setup in the ANSYS FE program, which allows running the three blocks with a relatively smooth flow of data between them. It has been found that 2-D elements provide almost identical accuracy at significantly less calculations (in this case over 20 times faster than the model with 3-D elements). A heat transfer in the direction perpendicular to the actuator's plane is included in the ANSYS' 2-D elements SHELL157, which were used within the electrical and thermal blocks. Next, the element SHELL63 was used within the mechanical block. In the areas where

large amounts of Joule heat is produced elements are smaller and placed more densely (Figure 7). A particular meshing of the FE model was considered accurate (the model accuracy) when it was found insensitive to increased number of elements.

All the three environments include temperature dependent material properties, and therefore are coupled. However, as mentioned before, the iteration loops running only the electrical and thermal block are required to obtain the temperature solution.
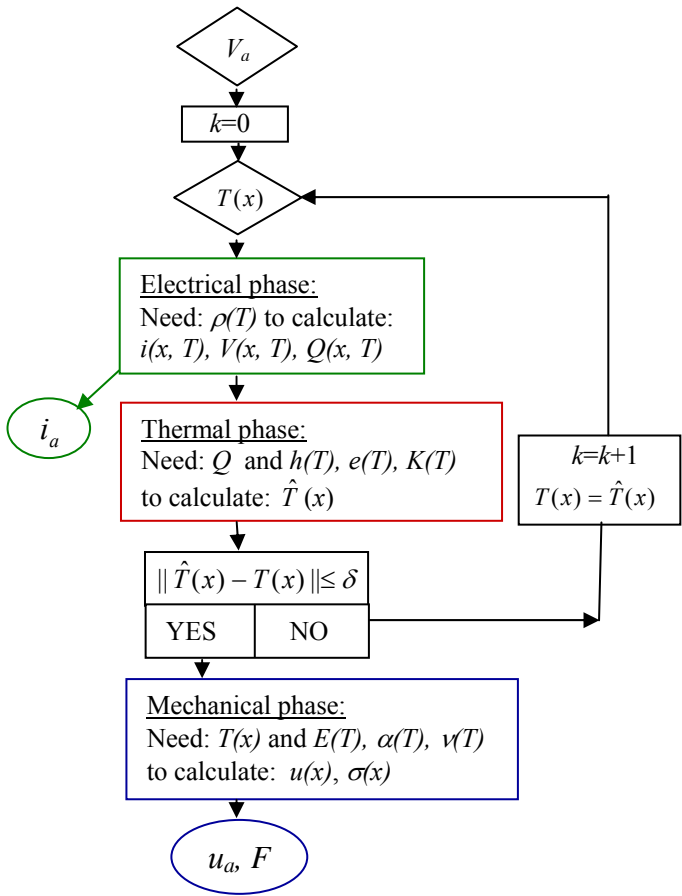

Figure 4:   Flow chart of the FE analysis.

To start the simulation, an external voltage V_a is applied across a cascaded actuation unit. Resistivity $\rho(x, T(x))$ at each point x of the actuator is calculated using an initially assumed (or calculated in the previous loop) temperature distribution $T(x)$. The electrical procedures are then used to obtain current

density $i(x,T)$, voltage $V(x,T)$ and the Joule heat energy $Q(x,T)$ distributions. The latter is sent to the block solving the heat transfer problem, in which a best guess of the value for η in Eqn. (7) is used. In this block the thermal properties such as convection $h(T(x))$, emissivity $e(T(x))$, conduction $K(T(x))$ are evaluated at the current temperature distribution $T(x)$.

With this information a new temperature distribution $\hat{T}(x)$ is calculated. If this new temperature is not within some preset convergence limits δ, then $\hat{T}(x)$ is substituted for $T(x)$ and the electrical and thermal analyses are repeated. Actually, it was solved by the standard Newton-Raphson in which the convergence was set in such a way that $\left\| i(x,\hat{T})/i(x,T)-1 \right\| < 0.001$ for the electrical block and $\left\| q(x,\hat{T})/q(x,T)-1 \right\| < 0.001$ for the thermal block (where q is the heat flux). Once a convergent temperature distribution is determined, the total current for the actuator i_a is calculated and the temperature field is sent to the mechanical block. This temperature is used to assign the values of such material constants as the elastic modulus $E(T(x))$, the thermal expansion coefficient $\alpha(T(x))$ to calculate the stress and displacement fields, which includes the displacement of the motion platform u_a.
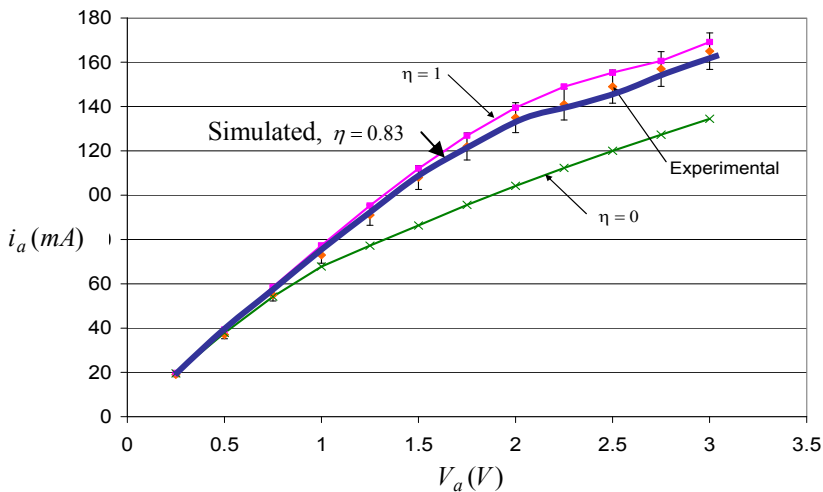

Figure 5:   The current match.

Note that the magnitude of this displacement depends on the values assigned to parameters $\alpha_0, \alpha_1, \alpha_2, \alpha_3, T_1, T_2$, and T_3 discuss before. If the platform motion is constrained then force F generated by the actuation unit to constrain it is calculated.

The real actuators are usually tested for the $i_a^{\exp}(V_a)$ and $u_a^{\exp}(i_a)$ relationships (see Figures 5 and 6).

In order to achieve as close an agreement as possible with these experimental result the parameters η, α_i, and T_i characterizing the material properties in the simulation presented in Figure 4 should be properly adjusted. Note that the difference $i_a - i_a^{\exp}$ depends only on the value of parameter η. The 'best' match for the voltage from $0.25V$ to $3.0V$ was obtained for $\eta = 0.83$ and is shown in Figure 5. Also included, for comparison, are the results when using $h_t(T)$ or $h_w(T)$. In turn, to minimize the difference $u_a - u_a^{\exp}$ the values of parameters α_i and T_i indicated in Figure 3 were modified. The best match is shown as a solid line in Figure 6.
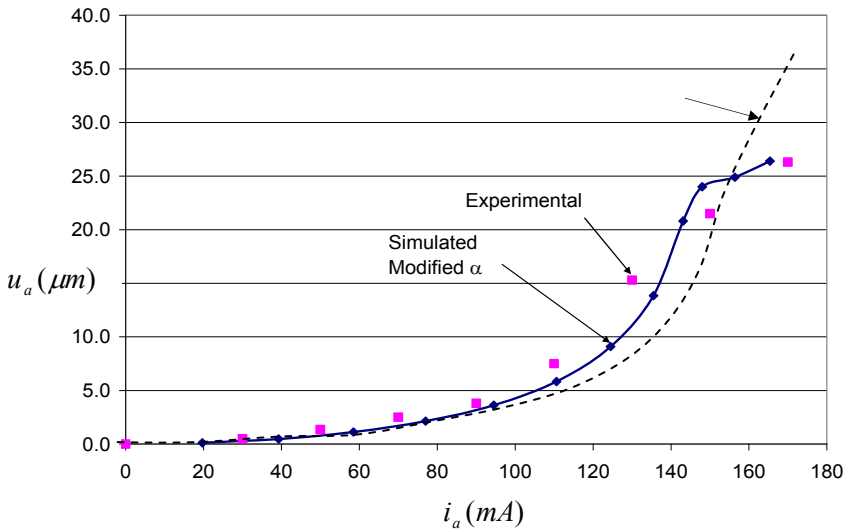

Figure 6:   The displacement match.

The displacement obtained by the applying the linear relation (9) for the thermal expansion coefficient is also shown, for comparison.

5   Other results of the simulation

The voltage distribution for $V_a = 0.63$ V is depicted in Figure 7a. The average voltage drop over an actuation cell is 0.09V. However, in the bottom cells a voltage drop is ~0.067V, while in the top cells a drop is ~0.093V. This unequal voltage distribution can be attributed to different temperatures of these cells (this is shown in Figure 7b). Bottom cells are cooler then the top cells due to

conduction of heat into the anchor. Since resistivity is lower in colder cells and the same current passes through each cell, the voltage drop is not uniform.

The corresponding temperature distribution is presented in Figure 7b. It should be noted that roughly half of the actuator's material undergone the transition phase occurring at $T_a = 306$ ºC.

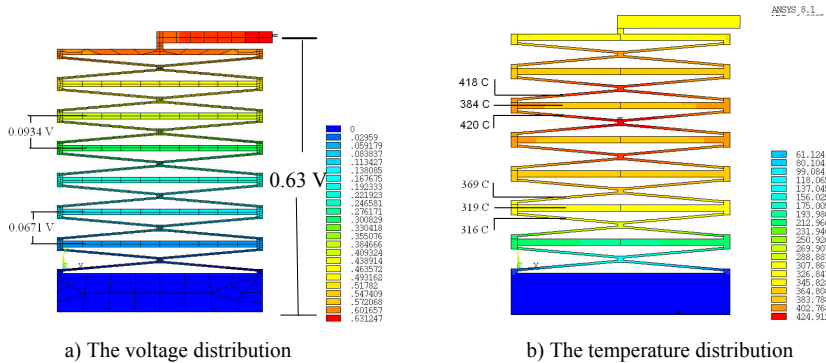

| a) The voltage distribution | b) The temperature distribution |

Figure 7:   The FE results.

On average the constrainers are cooler by about 35ºC than the hot arms. Closer analysis reveals that this difference is responsible for about 90% of the displacement generated by the unit at the motion platform

6   Conclusions

Detailed knowledge of the temperature dependency of several electro-thermal-mechanical material properties is necessary to accurately simulate the ETMA by the FE method. A great deal of caution should be exercised when selecting data from the literature, because some of these properties are very sensitive to a particular composition of the material. Also, some changes in the material internal structure may have significant effect on these properties. For example, the resistivity of the nickel alloys used in the ETMA presented varies quadratically below the temperature of the magnetic phase change, but linearly above it. Similarly, the conduction drops with temperature below the transition point, and increases above it.

The simulation results appear to be mostly affected by the uncertainty in the convection coefficient, the values of which may vary several times over the temperature range involved. This coefficient happens to be also scale dependant and impossible to measure accurately for the members of the actuator due to its small dimensions.

The 'uncertain' material characteristics can be 'tuned up' by combining the FE simulation with the experimental measurements of the ETMA performance. It should be noticed that the electrical and thermal characteristics should be adjusted simultaneously due to coupling, while the mechanical properties could be modified independently.

    The FE simulation procedure is iterative, runs across the three physics phenomena, and is computationally extensive. However, proper choices of elements, meshing patterns, and iterative schemes may substantially reduce the calculations and alleviate the convergence problems.

References

[1]   T. Moulton, G.K. Ananthasuresh. Micromechanical devices with embedded electro-thermal-compliant actuation. *Sensors and Actuators* A, 90, 2001, p 38-48.

[2]   D. Hill, W. Szyszkowski, and E. Bordachev, On Modeling and Computer Simulation of an Electro-thermally Driven Cascaded Nickel Micro-actuator*, Sensors and Actuators* A, 126, 2006, pp. 253-263.

[3]   C.P. Hsu, W.C. Tai, W. Hsu. Design and Analysis of an Electro-Thermally Driven Long-Stretch Micro Drive with Cascaded Structure. *Proceedings of IMECE2002*, 2002.

[4]   H. Du, C. Su, M. K. Lim, W. L. Jin. A micro-machined thermally-driven gripper: a numerical and experimental study. *Smart Mater. Struct*, 8, 1999, p. 616-622.

[5]   P. Lerch, C.K. Slimane, B. Romanowicz, P. Renaud. Modelization and characterization of asymmetrical thermal micro-actuators. *J. Micromech. Microeng*. 6, 1996, p 134-137.

[6]   N. Mankame, G.K. Ananthasuresh. Comprehensive thermal modeling and characterization of an electro-thermal-compliant microactuator. *J. Micromech. Microeng*. 11, 2001, p 452-462.

[7]   E.V. Bordatchev, S.K. Nikumb, and W. Hsu, Laser micromachining of the miniature functional mechanisms*, Proceedings of SPIE, Vol. 5578* (SPIE, Bellingham, WA, 2004), paper # 5578D-77, pp. 579-588.

[8]   King, J., *Materials Handbook for Hybrid MicroElectronics*. Artech House, Boston, 1988.

[9]   Everhart, J., *Engineering Properties of Nickel and Nickel Alloys*. Plenum Press, New York, 1971.

[10]   Temperature Dependent Elastic & Thermal Properties Database, MPDB (JAHM) Software, Inc., USA, 1999.

[11]   Yao, Y D, Tsai, J H. Magnetic Phase Transition in Nickel-Rich Nickel-Copper Alloys, *Chinese Journal of Physics*, Vol. 16, No 4. p. 189 – 195, 1978.

[12]   Incropera F.P. and Dewitt D.P. *Fundamentals of Heat and Mass Transfer*, Fifth Edition. John Wiley and Sons, New York, 2002.

[13]   T A Faisst. Determination of the critical exponent of the linear thermal expansion coefficient of nickel by neutron diffraction. *J. Phys.: Condens. Matter 1*, 1989, p 5805-5810.

[14]   T G Kollie. Measurement of the thermal-expansion coefficient of nickel from 300 to 1000 K and determination of the power-law constants near the curie temperature. *Physical Review B,* V16, N11, 1977, p 4872-4882.